# Supercritical CO2-assisted extrusion foaming: A suitable process to produce very lightweight acrylic polymer micro foams

Margaux Haurat, Martial Sauceau, Fabien Baillon, Louise Le Barbenchon, Matthieu Pedros, Michel Dumon

Received: 14 June 2022 | Revised: 12 October 2022 | Accepted: 15 October 2022

DOI: 10.1002/app.53277

RESEARCH ARTICLE

Applied Polymer SCIENCE WILEY

# Supercritical $CO_2$-assisted extrusion foaming: A suitable process to produce very lightweight acrylic polymer micro foams

**Margaux Haurat**[1] | **Martial Sauceau**[2] | **Fabien Baillon**[2] | **Louise Le Barbenchon**[3] | **Matthieu Pedros**[4] | **Michel Dumon**[1,4]

[1]Laboratoire de Chimie des Polymères Organiques, Université de Bordeaux, CNRS, Bordeaux INP/ENSCBP, UMR 5629, PessacCedex, France

[2]Centre RAPSODEE, UMR CNRS 5302, IMT Mines Albi, Université de Toulouse, Toulouse, France

[3]I2M Institut de Mécanique et Ingénierie - UMR CNRS 5295, Université de Bordeaux, Bordeaux, France

[4]Département Science et Génie Matériaux - SGM, IUT Université de Bordeaux, Bordeaux, France

**Correspondence**
Margaux Haurat, Laboratoire de Chimie des Polymères Organiques, Université de Bordeaux, CNRS, Bordeaux INP/ENSCBP, UMR 5629, Pessac Cedex, France.
Email: margaux.haurat@u-bordeaux.fr

**Funding information**
Agence Nationale de la Recherche, Grant/Award Number: AAPG PRCE 2018CE06 0030

## Abstract

A strategy of $CO_2$-assisted extrusion foaming of PMMA-based materials was established to minimize both foam density and porosities dimension. First a highly $CO_2$-philic block copolymer (MAM: PMMA-PBA-PMMA) was added in PMMA in order to improve $CO_2$ saturation before foaming. Then the extruding conditions were optimized to maximize $CO_2$ uptake and prevent coalescence. The extruding temperature reduction led to an increase of pressure in the barrel, favorable to cell size reduction. With the combination of material formulation and extruding strategy, very lightweight homogeneous foams with small porosities have been produced. Lightest PMMA micro foams ($\rho = 0.06$ g cm$^{-3}$) are demonstrated with 7 wt% $CO_2$ at 130°C and lightest blend micro foams ($\rho = 0.04$ g cm$^{-3}$) are obtained at lower temperature (110°C, 7.7 wt% $CO_2$). If MAM allows a reduction of $T^{foaming}$, it also allows a much better cell homogeneity, an increase in cell density (e.g., from 3.6 $10^7$ cells cm$^{-3}$ to 2 to 6 $10^8$ cells cm$^{-3}$) and an overall decrease in cell size (from 100 to 40 μm). These acrylic foams produced through $scCO_2$-assisted extrusion has a much lower density than those ever produced in batch ($\rho \geq 0.2$ g cm$^{-3}$).

**KEYWORDS**
acrylic polymer, extrusion foaming, foam, lightweight, $scCO_2$

## 1 | INTRODUCTION

In the huge field of porous materials, polymer foams are defined as biphasic products made of gaseous phases (named porosities, pores, or cells) separated by polymer walls.[1] Because of their light weight and multiple properties (e.g. thermal insulation, mechanical damping, acoustic insulation), thermoplastic foams are widely used.[2–4] The reduction of porosities dimension from micro to nano range is known as a challenge that could enhance foam performances (e.g. improve the thermal insulation because of Knudsen effect).[3] The foam structure control requires to consider polymer/blowing agent choice as a function of foaming process. In this study, extrusion foaming was selected because of its industrial relevance (high production rate, possibility to produce large foam parts). This process can be used to perform either chemical or physical foaming, distinguished by the type of blowing agent used.[5–8] Recently, chemical foaming was endangered by REACH regulation in Europe. The toxicity of some chemical blowing agents (CBA), necessary to release gases responsible of foaming (e.g., azodicarbonamide), was reported. Physical foaming, that consists in directly injecting the blowing agent in the extruder, can be safer.[7] Indeed, this route can be

performed with nontoxic, available and low-cost physical blowing agents (e.g., $CO_2$ or $N_2$) that ensure to not leave any toxic traces in the polymer after foaming. Supercritical carbon dioxide ($scCO_2$) is often selected as blowing agent because, in that state (reached above its critical point $P_C = 7.38MPa$ and $T_C = 31°C$), it presents a good solubility and diffusivity in polymers in comparison with other solvents, such as nitrogen.[9] Because of their good $CO_2$-philicity and processability, acrylic polymers are good candidates to $scCO_2$-assisted extrusion foaming.[5,10] Indeed, acrylics are the most $CO_2$-philic polymers after fluorinated polymers, hardly processable at high-temperature for HSE reasons.[2]

Already nano foamed in a discontinuous process (batch foaming), both poly(methyl methacrylate) (PMMA) and PMMA/10 wt% MAM blend were selected for $scCO_2$-assisted extrusion foaming.[11–13] In batch foaming, MAM triblock copolymer (PMMA-PBA-PMMA, where PBA is poly [butyl acrylate]) acts as $CO_2$-reservoirs due to the high $CO_2$-philicity of its central block.[14,15] Due to the nano structuration of the blend prior to foaming, MAM addition also tends to improve the foams porosity homogeneity and helps to reduce the mean cell size (e.g., $\emptyset_{cell\ PMMA} = 1900\,nm$ to $\emptyset_{cell\ PMMA/10\%MAM} = 96\,nm$ when saturated at 50 °C and 30 MPa for 16 h).[3] These results are encouraging, but the foam density is always around 0.2 $g\,cm^{-3}$.[14,16–18] Even if patents already exist on acrylics extrusion foaming assisted by $scCO_2$ stating the feasibility of extruded acrylic foams, the efficiency of MAM block copolymer to control foam structure in extrusion had never been proved before.[19]

Based on previous studies conducted on several polymers, a foaming strategy has to be established to control the foam structure in extrusion. In extrusion, the foaming steps, nucleation-growth, and coalescence, are launched by the phase separation induced by the depressurization at the extruder die. To limit the porosities dimensions, the extruder die temperature has to be lowered as much as possible; it causes an increase in the foaming pressure favorable to foam stabilization. To facilitate the extrusion of the polymer despite of the temperature decrease, the $CO_2$ flow rate can be increased to benefit of the plasticizing effect induced by the $scCO_2$ injection.[19,20]

This study aims to proof the efficiency of MAM triblock copolymer addition in PMMA to reduce the size and the density of extruded foams porosities.

## 2 | EXPERIMENTAL SECTION

### 2.1 | Materials

Neat poly(methyl methacrylate) (PMMA) and MAM triblock copolymer—poly(methyl methacrylate)-b-poly (butyl acrylate)-b-poly(methyl methacrylate)—pellets were supplied by Arkema (Lacq, France). Details on these materials findable in the literature are summarized in Table 1.[17,18,21] Carbon dioxide N27 (purity 99.7%), used as a foaming agent in this study, was supplied by LINDE.

Differential scanning calorimetry (DSC) was performed to determine thermal properties of each material used in this study. All the DSC measurements were performed on a TA Instrument device (Q100 RCS) at 20°C $min^{-1}$.

### 2.2 | Unfoamed blend preparation

A PMMA/10 wt% MAM blend was prepared by CANOE (Pau, France). First, PMMA and MAM pellets were dried at 80°C during 4 h in an oven. Then 90 wt% PMMA and 10 wt% MAM were dry blended in a cement mixer. Then, PMMA/10 wt% MAM pellets were introduced in a corotative twin extruder (Labtech $\emptyset = 26\,mm$, $L/D = 40$) in order to obtain a homogeneous blend. This blend was compounded with a temperature profile ranging from 250 to 230°C at a screw speed of 300 rpm. After the extruder die ($\emptyset = 3\,mm$), the rod was pelletized by a cutting machine and transparent pellets were produced.

**TABLE 1** Characteristics of the additives used in a PMMA matrix

| Commercial material name | State at room temperature | $M_n$ ($g\,mol^{-1}$) | $M_w$ ($g\,mol^{-1}$) | Tg[a] (°C) | Other characteristics | Density ($g\,cm^{-3}$) | Aspect |
|---|---|---|---|---|---|---|---|
| PMMA V825T clear 101 (Arkema, Lacq, France) | Glassy amorphous solid | 43,000 | 83,000 | 115.8 | Use as polymer matrix | 1.19 | Transparent |
| MAM M53 (Arkema, Lacq, France) | Rubbery center block + Glassy end-blocks | 82,000 | 128,000 | −44.4 (PBA) 113.5 (PMMA) | Triblock copolymer PMMA-PBA[b]-PMMA 54 wt% PBA | 1.03 | Transparent |

[a]Measured by DSC following (Figure 1).
[b]PBA: poly(butyl acrylate).

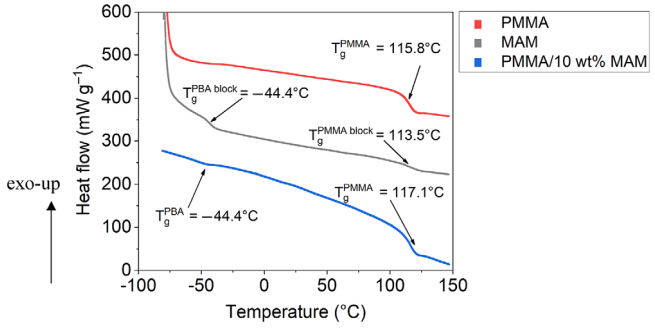


**FIGURE 1** Differential scanning calorimetry (DSC) of acrylic polymers and blend: PMMA, MAM, and PMMA/10 wt% MAM blend [Color figure can be viewed at wileyonlinelibrary.com]

## 2.3 | scCO$_2$-assisted extrusion foaming

Acrylic foams were produced through a scCO$_2$-assisted extrusion-foaming process at IMT Mines Albi (Albi, France). The foaming experiments were performed on a single-screw extruder (Rheoscam, Scamex) adapted with a CO$_2$ injection point located in the middle of the barrel. This device, schematized in Figure 1, has already been described in previous publications.[22–27]

This single-screw extruder has a screw diameter of 30 mm and a length to diameter ratio of 37. At the end of the extruder line, a removable static mixer was added in order to enhance distributive mixing of CO$_2$ in the polymer melt. This additional part, made of four elements with a diameter of 17 mm (SMB-H-17/4, Sulzer), also leads to improve both CO$_2$ sorption and dissolution in the polymer melt. After the static mixer, the set-up ends-up with a capillary die of 3 mm diameter and 12 mm length. Six heaters are distributed all along the barrel to ensure temperature regulation. As shown in Figure 2, two heaters are located before the CO$_2$ injection to control both $T_1$ and $T_2$. Than two heaters are following to control $T_3$ and $T_4$ after the CO$_2$ injection point. The temperature of the static mixer, $T_5$, and the temperature of the extruder die, $T_6$, are also controlled with heaters. Three temperature sensors are distributed along the extruder: $T_{mat_1}$ before the second gasight ring, $T_{mat_2}$ before the static mixer and $T_{mat_3}$ by the die. The pressure in the extruder is not directly controlled but induced by the temperature, the amount of CO$_2$ injected and its solubility in the polymer melt (Figure 3). The pressure in the extruder is measured in four different locations distributed along the barrel: $P_1$ after the CO$_2$ injection point, $P_2$ before the second gasight, $P_3$ before the static mixer and $P_4$ by the die. The maximum available pressure in the barrel is about 35 MPa; above this maximum pressure, the equipment shuts down. At the end of this set-up, the pressure drop rate (PDR) is about 100 MPa s$^{-1}$. Batch processes provide more commonly PDR of 0.33 to 3 MPa s$^{-1}$.[14,21] In this study, the screw speed (N) was fixed at 30 rpm. Below 30 rpm, the shearing is not sufficient and the CO$_2$ cannot be well mixed with the polymer blend.

Carbon dioxide, pumped from a cylinder by a syringe pump (260D, ISCO), is injected in the extruder at $L/D = 20$ (from the feed hopper). It is always injected at a pressure slightly superior or equal to the extruder pressure in order to prevent any gas return in the injector. During CO$_2$ injection, the syringe pump runs in a constant volumetric flow rate ($\dot{V}_{CO_2}$). In order to calculate the polymer mass flow rate ($\dot{m}^m_{polymer}$), samples extruded during a given period (generally 1 min) were collected at the end of the extruder and weighted. The CO$_2$ mass fraction ($w_{CO_2}$, in %) can be calculated following Equation (1):

$$w_{CO_2} = \frac{\dot{V}_{CO_2} \times \rho^{pump}_{CO_2}}{\dot{V}_{CO_2} \times \rho^{pump}_{CO_2} + \dot{m}^m_{polymer}} \times 100 \quad (1)$$

where $\dot{V}_{CO_2}$ is the syringe pump constant volumetric flow rate, $\rho^{pump}_{CO_2}$(g ml$^{-1}$) is the CO$_2$ density in the syringe pump at 5°C and at the injection pressure in the pump ($P_1$). This value, calculated with the Span and Wagner equation of state, is available on NIST website.[28,29]

As detailed in Table 2, for PMMA and PMMA/10 wt% MAM extrusion foaming experiments, the temperature was kept constant in the first heating zones ($T_1$ to $T_3$), where the polymer melts. The temperatures of the following heating zones ($T_4$ to $T_6$) were slightly decreased. With the temperature lowering, the CO$_2$ mass uptake increases in the polymer melt and the foam structure is quickly fixed at the die exit (*i.e.*, the coalescence is limited).[19,30,31]

To balance the increase of viscosity due to the temperature decrease and to take advantage of the CO$_2$ plasticizing effect, the CO$_2$ volumetric flow rate ($\dot{V}_{CO_2}$) is increased on the syringe pump.

For each ($P$, $T$) stabilized conditions, a foam sample extruded in 1 min was collected at the die exit. Each sample was named as follow: Material_T$_6$_$\dot{V}_{CO_2}$; where material is either PMMA or PMMA/10 wt% MAM. These extrudates porous samples were characterized in order to establish a link between processing conditions and foam structure, expansion, and density.

For both PMMA (Table 3) and PMMA/10 wt% MAM (Table 4) extrusion foaming, experiments were performed reducing the temperature until the maximum of pressure bearable by the extruder ($P_{max} \approx 35 MPa$) is reached.

In the specific case of pure PMMA extrusion (Table 3), the die temperature ($T_6$) was decreased up to 130°C at a

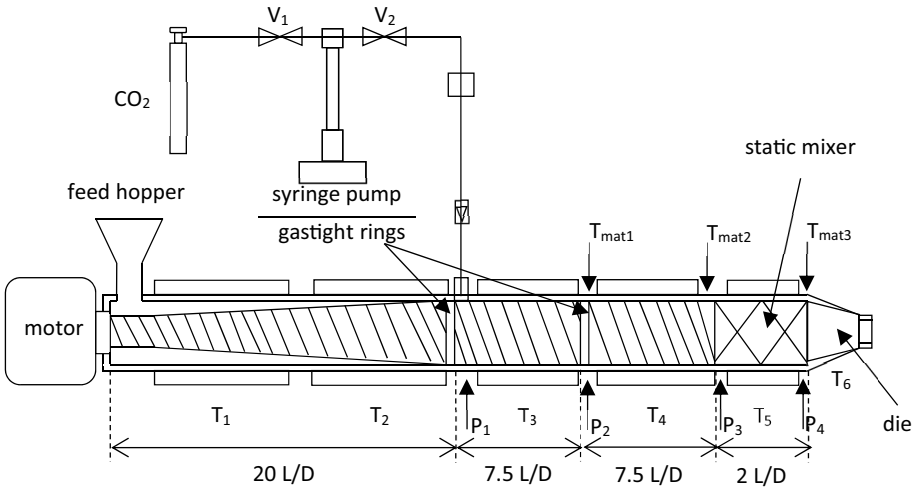


FIGURE 2 Schematic of the scCO$_2$-assisted single-screw extruder used to produce foams[22–27]

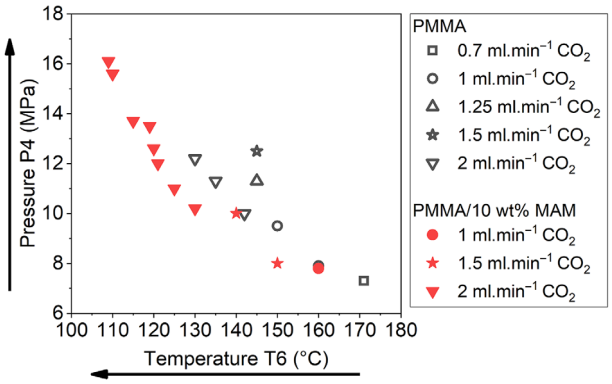


FIGURE 3 Pressure at the end of the extruder barrel as a function of extruder die temperature when foaming acrylic polymers (PMMA and PMMA/10 wt% MAM blend) with scCO$_2$ [Color figure can be viewed at wileyonlinelibrary.com]

TABLE 2 PMMA and PMMA/10 wt% MAM extrusion foaming conditions

| Processing conditions | PMMA | PMMA/10 wt% MAM |
|---|---|---|
| T1 (°C) | 210 | 210 |
| T2 (°C) | 250 | 250 |
| T3 (°C) | 230 | 230 |
| T4 (°C) | 190–230 | 150–200 |
| T5 (°C) | 137–171 | 113–160 |
| T6 (°C) | 130–171 | 109–160 |
| $\dot{V}_{CO_2}$ (ml min$^{-1}$) | 0.7–2 | 1–2 |
| N (rpm) | 25–40 | 30–40 |

CO$_2$ flow rate of 2 ml min$^{-1}$ (≈ 7 wt% CO$_2$ solubilized in the polymer). Close to 130°C, it was harder to homogenize the flux: the stabilization duration was longer and the polymer rod shows some tortuosity. Moreover, when the CO$_2$ flow rate is too high (it increases while the temperature decreases), CO$_2$ is not well solubilized in the polymer melt. Indeed, it creates some gas pockets that randomly burst at the die exit. These gas pockets indicate that the polymer is already saturated and additional gas amount is hardly soluble in the polymer melt with this set-up. In this study, the maximum amount of CO$_2$ solubilized in PMMA was roughly equal to 7 wt% CO$_2$.

In the case of PMMA/10 wt% MAM extrusion foaming (Table 4), the die temperature ($T_6$) was decreased up to 109°C at a CO$_2$ flow rate of 2 ml min$^{-1}$. Below 109°C, the device stopped and the limit of pressure was reached (35 MPa). For the blend, the limit of pressure (35 MPa) was reached at a lower temperature (109°C) than for pure PMMA (130°C). The MAM addition in pure PMMA matrix caused a slight decrease of viscosity (Figure 9, Data S1) and an increase of CO$_2$-philicity.[31] Thus, during blend foaming, both MAM and CO$_2$ act as plasticizers and help to temperature lowering.

## 2.4 | Characterization techniques

### 2.4.1 | Density

Unfoamed materials apparent density $\left(\rho_S^{H_2O},\ \mathrm{g\ cm^{-3}}\right)$ g cm$^{-3}$ and foams apparent density $\left(\rho_f^{H_2O},\ \mathrm{g\ cm^{-3}}\right)$ were determined with a water pycnometer following the water displacement method. Based on Archimede's principle, one can determine the apparent density of a sample $\left(\rho_{sample}^{H_2O},\ \mathrm{g\ cm^{-3}}\right)$ following Equation (2):

$$\rho_{sample}^{H_2O} = \frac{m_{dry\ sample}}{m_{dry\ sample} + \Delta m} \times \rho_{H_2O} \quad (2)$$

where $m_{drysample}$ (g) is the sample mass, $\Delta m$ (g) is the mass loss between the water filled pycnometer ($m_{pycno+H_2O}$, g) and the water filled pycnometer containing the sample ($m_{pycno+H_2O+sample}$) as written in Equation (3) and $\rho_{H_2O}$ is the density of water ($\rho_{H_2O} = 1\,g\,cm^3$):

**TABLE 3** Neat PMMA foams extruded at given conditions and collected at the extruder die exit

| Sample name | $T_6$ (°C) | $\dot{V}_{CO_2}$ (ml min$^{-1}$) | $\dot{m}^m_{polymer}$ (g min$^{-1}$) | $\rho^{pump}_{CO_2}$ (g ml$^{-1}$) | $w_{CO_2}$ (%) |
|---|---|---|---|---|---|
| PMMA_170_0 | 170 | 0 | - | - | 0 |
| PMMA_171_0.7 | 171 | 0.7 | 56.0 | 0.9964 | 1.2 |
| PMMA_160_1 | 160 | 1 | 52.9 | 1.0032 | 1.9 |
| PMMA_150_1 | 150 | 1 | 51.0 | 1.0007 | 1.9 |
| PMMA_145_1.25 | 145 | 1.25 | 50.0 | 1.0155 | 2.5 |
| PMMA_145_1.5 | 145 | 1.5 | 50.9 | 1.0207 | 2.9 |
| PMMA_142_2 | 142 | 2 | 51.0 | 1.0305 | 3.9 |
| PMMA_135_2 | 135 | 2 | 42.7 | 1.0421 | 4.6 |
| PMMA_130_2 | 130 | 2 | 27.0 | 1.0526 | 7.2 |

**TABLE 4** PMMA/10 wt% MAM blend foams extruded at given conditions and collected at the extruder die exit

| Sample name | $T_6$ (°C) | $\dot{V}_{CO_2}$ (ml min$^{-1}$) | $\dot{m}^m_{polymer}$ (g min$^{-1}$) | $\rho^{pump}_{CO_2}$ (g ml$^{-1}$) | $w_{CO_2}$ (%) |
|---|---|---|---|---|---|
| PMMA/10 wt% MAM_160_0 | 160 | 0 | - | - | 0 |
| PMMA/10 wt% MAM_160_1 | 160 | 1 | 43.2 | 1.0023 | 2.3 |
| PMMA/10 wt% MAM_150_1.5 | 150 | 1.5 | 47.9 | 1.0085 | 3.1 |
| PMMA/10 wt% MAM_140_1.5 | 140 | 1.5 | 33.6 | 1.0147 | 4.3 |
| PMMA/10 wt% MAM_130_2 | 130 | 2 | 28.0 | 1.0328 | 6.9 |
| PMMA/10 wt% MAM_125_2 | 125 | 2 | 27.2 | 1.0338 | 7.1 |
| PMMA/10 wt% MAM_121_2 | 121 | 2 | 31.6 | 1.0374 | 6.2 |
| PMMA/10 wt% MAM_120_2 | 120 | 2 | 32.1 | 1.0430 | 6.1 |
| PMMA/10 wt% MAM_119_2 | 119 | 2 | 31.4 | 1.0517 | 6.3 |
| PMMA/10 wt% MAM_115_2 | 115 | 2 | 31.7 | 1.052 | 6.2 |
| PMMA/10 wt% MAM_110_2 | 110 | 2 | 32.0 | 1.0563 | 6.2 |
| PMMA/10 wt% MAM_109_2 | 109 | 2 | 25.0 | 1.0577 | 7.7 |

$$\Delta m = m_{pycno+H_2O} - m_{pycno+H_2O+sample} \quad (3)$$

Three measurements were performed for each sample and the mean value is given here.

Foams density were also measured with a helium pycnometer $\left(\rho_f^{He},\ \mathrm{g\ cm^{-3}}\right)$ (Thermofisher Pycnomatic ATC) at CANOE (Pau, France) in order to determine the porosity and the expansion of each sample as detailed in the next paragraphs. Three measurements were performed for each sample and the mean value is given here.

### 2.4.2 | Porosity

The total foam porosity ratio ($\varepsilon_{T,}$), can be determined following Equation (4):

$$\varepsilon_T = \frac{V_{total\ porosity}}{V_{total}} = 1 - \frac{\rho_f^{H_2O}}{\rho_S^{H_2O}} \quad (4)$$

where $\rho_f^{H_2O}$ is the apparent foam density and $\rho_S^{H_2O}$ is the apparent solid material density (before foaming).

The open porosity ratio ($\varepsilon_O$) of each sample as determined following Equation (5), as described by Chauvet et al.[22]:

$$\varepsilon_O = \frac{V_{open\ porosity}}{V_{total}} = 1 - \frac{\rho_f^{H_2O}}{\rho_f^{He}} \quad (5)$$

where $\rho_f^{He}$ is the apparent foam density measured with a helium pycnometer. Once foam total porosity and open porosity have been determined, it is possible to calculate the open-cell content (OC), following Equation (6):

$$OC = \frac{\varepsilon_O}{\varepsilon_T} \quad (6)$$

### 2.4.3 | Expansion

The total expansion ($E_T$) of each sample was determined following the Equation (7):

$$E_T = \frac{\rho_S^{H_2O}}{\rho_f^{H_2O}} = \frac{1}{1-\varepsilon_T} \quad (7)$$

Depending on its $CO_2$ content, each sample can reach a specific maximum expansion ratio ($E_T^{max}$).[32] When $E_T^{max}$ is calculated the following hypothesis is made: all the injected blowing agent contributes to foaming. This value can be approximated following Equation (8), making the hypotheses that $CO_2$ does not escape from the sample and all the gas is used for expansion[33]:

$$E_T^{max} = \frac{V_{polymer} + V_{CO_2}^{amb}}{V_{polymer}} = 1 + \frac{w_{CO_2}}{1-w_{CO_2}} \times \frac{\rho_S^{H_2O}}{\rho_{CO_2}^{amb}} \quad (8)$$

where $w_{CO_2}$ is the $CO_2$ mass fraction in the sample, $\rho_S^{H_2O}$ the apparent solid material density (before foaming) and $\rho_{CO_2}^{amb}$ the $CO_2$ density in room pressure and temperature conditions. As given in the literature tables, at room conditions, $\rho_{CO_2}^{amb} = 1.78 \text{kgm}^{-3}$.[29]

### 2.4.4 | Cellular structure

The foams cellular structure was observed with a scanning electron microscope (SEM) Zeiss EVO HD 15 at I2M (Université de Bordeaux, France). Before SEM observation, the samples were fractured in liquid nitrogen to avoid structure distortions. The samples, fractured perpendicularly to the extrusion direction, were then gold coated with a sputter coater. Acrylic foams were observed with a SEM at 10 kV (to not destroy the foam structure with the electron beam) and at a working distance $WD \approx 10\,\text{mm}$ in secondary electron (SE) mode. The obtained micrographs were analyzed with Piximètre (version 5.10) to measure mean cell size ($\emptyset_{cell}$). After image analysis and densities measurements, it is possible to evaluate the number of cells per cubic centimeter ($N_C$) of dense material following Equation (9)[34]:

$$N_C = \frac{6\left[\left(\rho_S^{H_2O}/\rho_f^{H_2O}\right) - 1\right]}{\pi(\emptyset_{cell})^3} \quad (9)$$

where $N_C$ is expressed in cells $\text{cm}^{-3}$, $\rho_S^{H_2O}$ is the apparent solid material density (before foaming) and $\rho_f^{H_2O}$ is the apparent foam density and $\emptyset_{cell}$ is the mean cell size (cm).

## 3 | RESULTS AND DISCUSSION

### 3.1 | Strategy of $CO_2$ extrusion for very lightweight foams with small pores

When the objective is to fabricate very low-density foams (whatever the polymer type, such as PP, HIPS, PS[32,35,36]) with very small pore-size by continuous extrusion $CO_2$ foaming, at least three key factors should be achieved[2,30,33,35]:

1. Reach the highest possible pressure in the extruder, to enhance expansion (and nucleation),
2. Set the lowest possible die temperature to quickly vitrify the foam and prevent growth and coalescence,
3. Solubilize the highest possible amount of $CO_2$ in the polymer, to enhance the total expansion ratio ($E_T$) and to lower the foam density.

For PMMA and PMMA/10 wt% MAM blend foaming, the extruding temperatures were lowered (to cause an increase of pressure) while the amount of $CO_2$ injected was injected. The acrylic foams produced were characterized and their density were plotted as a function of extruder die temperature ($T_6$) in Figure 4 showing a stable very low minimum density.

Before foaming, dense PMMA had a density $\rho_S^{H_2O} = 1.19 \text{gcm}^{-3}$ while the lightest PMMA foam extruded (at 130°C at the die exit and at 7.2 wt% $CO_2$; solubilized in PMMA) has a density $\rho_f^{H_2O} = 0.06 \text{gcm}^{-3}$. From 170 to 130°C at 0.7–2 ml $\text{min}^{-1}$ $CO_2$, PMMA foam density

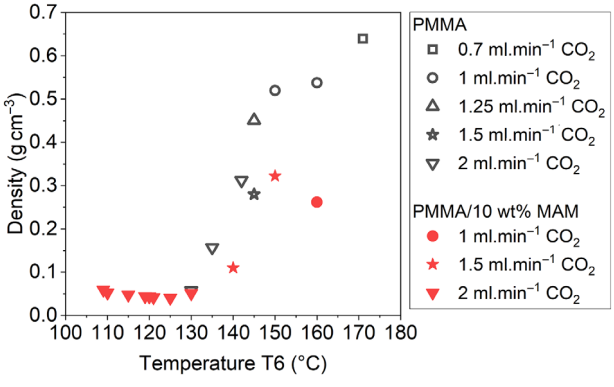


**FIGURE 4** PMMA and PMMA/10 wt% MAM foams densities (measured with water pycnometer) as a function of extruding temperature and $CO_2$ injected [Color figure can be viewed at wileyonlinelibrary.com]

decreased with the temperature. At 130°C, the device stopped due to a pressure increase (up to the device limit of pressure, 35 MPa) in the extruder. With this limit, the condition (1) of maximizing pressure near the die (see beginning of results section) is fulfilled with our experimental set-up.

Before foaming, dense PMMA/10 wt% MAM blend has a density $\rho_S^{H_2O} = 1.18 g cm^{-3}$ while the lightest foam obtained in extrusion-foaming (at 125°C at the die exit and at 2 ml $min^{-1}$ $CO_2$; *i.e.* 7 wt% solubilized in the polymer) has a density $\rho_f^{H_2O} = 0.04 g cm^{-3}$. Despite of their very low density the maximum expansion was not reached. As an example, PMMA/10 wt% MAM_125_2 expansion ($E_T$) was close to 30 while it could theoretically reach a maximum expansion ($E_T{}^{max}$) of 51. This difference is due to $CO_2$ gas escapes from the sample and gas pockets that do not contribute to foaming.

For the blend, from 160 to 130°C, the density decreases with the die temperature ($T_6$). Then, when the die temperature was reduced from 125 to 109°C, the density reached a plateau $\left(\rho_f^{H_2O} \approx 0.04 g\,cm^{-3}\right)$. This limit in density reduction is caused by a geometric effect called "limited cell packing."[20] Indeed, despite of the processing conditions optimization, the density cannot be indefinitely reduced. Even if the porosities diameter is reduced, denser domains still separate the different spherical cells. These denser gaps maintain a limit of density, as observed in Figure 4. Regardless of the density plateau $\left(\rho_f^{H_2O} \approx 0.04 g.cm^{-3}\right)$ reached for blend foams, the die temperature was further reduced until the pressure limit was reached (35 MPa).

Thus, in the following paragraphs, the temperature effect on foams morphology and density was studied.

In comparison with batch foaming, the lightest PMMA foam produced in this study (e.g., $\rho_f^{H_2O} = 0.06 g\,cm^{-3}$ when $T_6 = 130°C$ at 2 ml $min^{-1}$ $CO_2$) is close to 10 times lighter than the lightest PMMA foam produced, at present, in batch by Pinto et al. $\left(\rho_f^{H_2O} = 0.46 g\,cm^{-3}\right.$ foamed at $P_{sat} = 30 MPa$; $T_{sat} = 23°C$; $t_{sat} = 24 h$; $\left.{}^{\Delta P}/_{\Delta t} = 30 MPa.min^{-1}\right)$.[14] In the case of PMMA/10 wt% MAM, the lightest foam produced ($\rho_f^{H_2O} = 0.04 g\,cm^{-3}$ when foamed at 125°C at the die exit and at 2 ml $min^{-1}$ $CO_2$) is also 10 times lighter than the lightest foam obtained, at present, in batch by Reglero et al. $\left(\rho_f^{H_2O} = 0.4\ cm^{-3}\right.$ obtained at $P_{sat} = 30$ MPa; $T_{sat} = 20°C$; $\left.t_{sat} = 16 h; {}^{\Delta P}/_{\Delta t} = 15 MPa\ min^{-1}\right)$.[37] Guo et al. have produced nanocellular foams ($\emptyset_{cell} = 20$ nm) in two-step batch foaming saturating their samples at very low temperature (up to −30°C) to increase the $CO_2$-solubility in the polymer.[38]

Costeux et al. also produced acrylic (PMMA-based) foams in $scCO_2$-assisted extrusion foaming.[30] These authors set a special extrusion $CO_2$ line in which different equipment separate stages with different equipment: (i) melting (in the extruder), (ii) mixing (in a mixer at the $CO_2$ inlet), (iii) cooling (in a cooler of specific design, either parallel slots or static mixer) in order to enhance the $CO_2$ dissolution and to improve the polymer saturation and foaming by maintaining the pressure. With this set-up and an optimization of processing conditions, they have produced a pure PMMA foam with a density of 0.036 g $cm^{-3}$ (when 4.8 wt% $CO_2$ was dissolved in the polymer melt and when the die was at 133°C). The PMMA smallest density they reached is in the same order of magnitude as the results obtained in our study.

Now, nucleation density and pore size should be compared, thus foams morphologies are analyzed.

## 3.2 | Evolution of total expansion and total porosity

For each collected sample, both total porosity ratio ($\varepsilon_T$) and total expansion ($E_T$) were calculated following Equation (4) and Equation (7). Then, $\varepsilon_T$ and $E_T$ have been respectively plotted as a function of die temperature ($T_6$) in Figure 5.

Starting with PMMA foaming at high temperature (170°C and 0.7 ml $min^{-1}$ $CO_2$), a foam with 45%

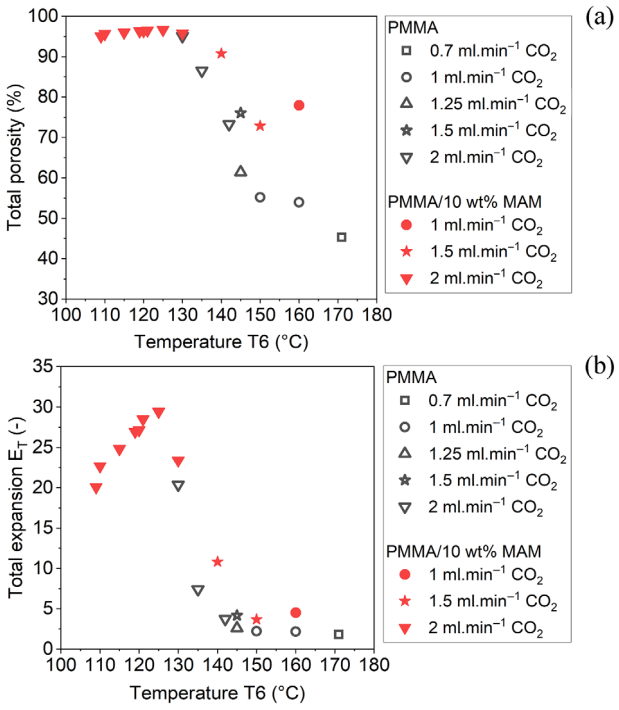


FIGURE 5 PMMA and PMMA/10 wt% MAM foams total porosity (a) and total expansion (b) as a function of die temperature ($T_6$) and $CO_2$ injection speed [Color figure can be viewed at wileyonlinelibrary.com]

total porosity ($\varepsilon_T$) is produced. When the die temperature is lowered down to 130°C (and 2 ml min$^{-1}$ $CO_2$) the foam total porosity has more than doubled (reaching 95%). When this maximum of total porosity is reached, the optimum of PMMA foam expansion is also reached ($E_T = 20$).

PMMA/10 wt% MAM foams produced in presence of $CO_2$, foamed from 160°C (and 1 ml min$^{-1}$) to 109°C (and 2 ml min$^{-1}$), have a total porosity ranging from 78% (at 160°C) to 97% (at 125°C).

Both PMMA and PMMA/10 wt% MAM foams produced when the die temperature reached 130°C, are highly porous (≥90%). Even if the same range of total porosity was reached for both neat PMMA and PMMA/10 wt% MAM at given (*P, T*) extruding conditions, the samples have different morphologies (Figure 4 and Figure 5) and do not have the same total expansion. Indeed, the pure PMMA foams did not expand as much as the PMMA/10 wt% MAM foams. For a given die temperature and $CO_2$ flow rate (e.g., at 130°C and 2 ml min$^{-1}$ $CO_2$), PMMA/10 wt% MAM sample has an expansion of $E_T = 23$ while pure PMMA has a total expansion $E_T = 20$. In the blend, the presence of MAM facilitates the material expansion and shaping due to its very low glass transition temperature ($T_g = -44.4$°C). Thus, a maximum of expansion $E_T \approx 29$ was reached when the die temperature was set at 125°C. Moreover, the PMMA corona of MAM $CO_2$ reservoirs prevent gas escape during the blend foaming. By this way, the gas can play its role of foaming agent for a longer duration than in pure PMMA, where the gas tends to escape because it is not constrained in that type of domains.

The PMMA/10 wt% MAM total expansion curve (Figure 5b) exhibits a maximum. This trend has already been observed by Naguib et al. for poly(propylene) (PP) foams extrusion in presence of $CO_2$ and by Chauvet et al. for poly(lactic acid) (PLA).[28,36] As described in their articles, two mechanisms are governing the expansion: (i) at high temperatures, down to a maximum of expansion upon decreasing the temperature, total expansion is governed by gas loss and (ii) when the temperature is reduced below the temperature of maximum expansion, expansion is directly linked to the material solidification.

1. On the high temperature side (from 160 to 125°C in PMMA/10 wt% MAM, in this study), the $CO_2$ has a high diffusivity and escapes from the material at the die exit. Thus, its contribution to expansion is low and the material expansion is limited (e.g., at 160 and 150°C). When the die temperature decreases $CO_2$-diffusivity in the polymer decreases and gas losses are limited so $CO_2$ is kept in the material to contribute to foam expansion.
2. On the low temperature side (*i.e.* below 125°C in this study), the material vitrifies quickly and the foam structure is rapidly frozen. When the temperature is reduced below the foam expansion optimum (e.g., below 125°C in this study), the foam structure is so rapidly frozen that the gas cannot fully contribute to material expansion. In that case, the effect of solidification is stronger than the gas contribution to expansion.

In the case of pure PMMA, we did not obtain a bell curve due to processing and material limitations. Indeed, with our set-up, it was not possible to cool the material below 130°C without reaching the maximum of pressure of our extruder (35 MPa).

## 3.3 | Foams structure and morphology

### 3.3.1 | Pure PMMA foams morphology

As shown in Figure 6, at 171°C, pure PMMA foam contains large cells. The porosities observed in PMMA_171_0.7 tend to be spherical and generally have homogeneous dimensions ($\emptyset_{cell} \approx 140\,\mu m$). Because cells dimensions are fixed when the growth and coalescence are stopped, (i.e., when the material cools down and vitrifies) lowering the die temperature ($T_6$) is a way to produce foams with smaller cells. This trend was observed down to 142°C. Below 142°C, apparent mean pore diameter increases again, but one can distinguish two types of spherical porosities (e.g., "large," $\emptyset_{large\ cell} \approx 200\,\mu m$ and "small," $\emptyset_{small\ cell} \approx 50\,\mu m$ in PMMA_130_2 sample). This bimodality has already been observed in other polymer foams produced through extrusion foaming (e.g., PMMA; poly[styrene] foams).[30,39,40] Costeux et al. linked this bimodality to an inefficiency of $CO_2$ dissolution in the polymer melt at given (P, T, $w_{CO_2}$) conditions; also related to the observed fact that the expansion ratio is not maximum ($E_T \neq E_T^{max}$).[30]

As shown in Figure 4, all the PMMA foams produced through continuous process in this study are microcellular. A discontinuous process makes possible to choose independently saturating pressure, temperature, and foaming time. In extrusion foaming, despite of the material ability to nanofoam, homogeneous nano foams are hardly achievable due to the high processing temperatures. Finally, opposite to batch foaming, the polymer residence time is limited in extrusion foaming process. If too short (i.e., when the screw speed is too high), the $CO_2$ cannot be well solubilized in the polymer and the flow is unstable. If too long (i.e., when the screw speed is too low), at high temperature PMMA is subjected to

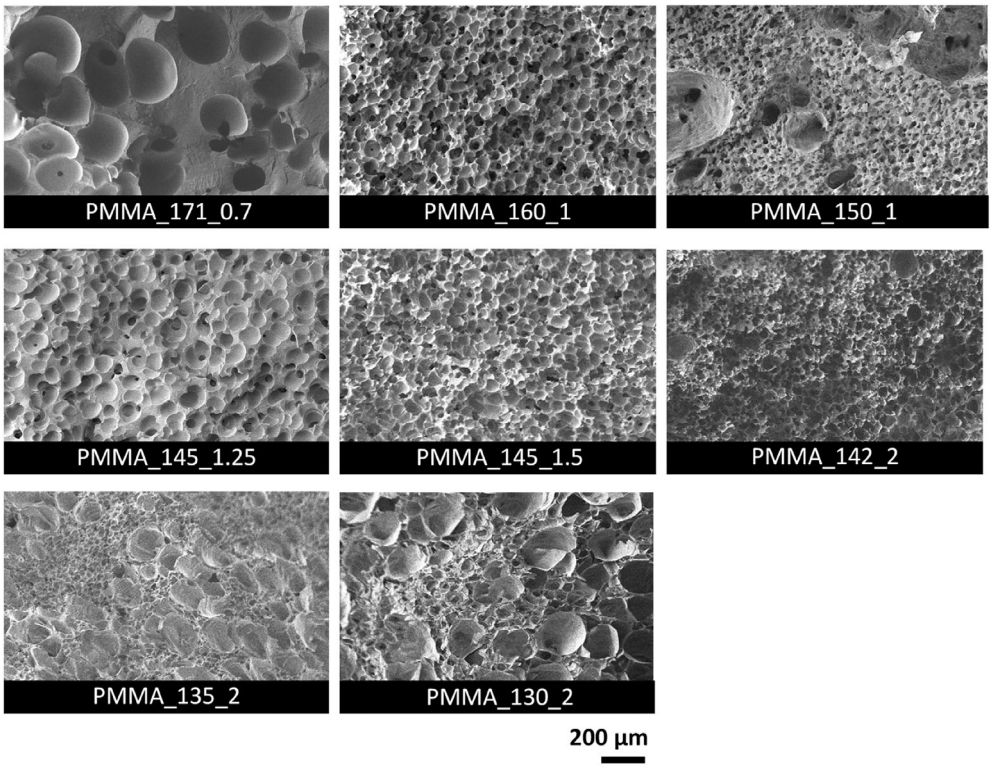


**FIGURE 6** SEM images (X200) of central area of neat PMMA foams extruded in conditions detailed in Table 3

degradation. When shearing is limited, $CO_2$ is not well solubilized in the polymer. Costeux et al. added a cooler before the extruder die to increase the residence time and reach lower temperatures.[30] With this additional element and a set-up slightly different (e.g., $CO_2$-injection point closer to the die exit), they produced sub-micro foams ($\emptyset_{cell} = 310$ nm) obtained when the cooler was set at $T =$ 38°C and reached $P = 36$ MPa with 23.1% $CO_2$ dissolved in the PMMA/$CO_2$ mixture.

In our study with a simpler equipment, the temperature effect was scanned and the condition (2) (see beginning of results section) of lowering temperature, near the die, is fulfilled with our experimental set-up and choice of material system. Note that block copolymer MAM did allow a great reduction in extrusion temperature. Finally looking at the whole extrudates, one interesting point is that nearly no skin is obviously present around the extrudates.

### 3.3.2 | PMMA/10 wt% MAM foams morphology

In batch foaming, MAM was added into PMMA matrix to greatly increase cell density and reduce mean cell size. In this study, the same strategy was followed to improve PMMA extrusion foaming and morphology control. As shown in Figure 7, at 160°C, PMMA/10 wt% MAM foam is homogeneous ($\emptyset_{cell} \approx 40$ µm) and contains spherical cells separated by thick cell walls (≈ 2 µm).

When the die temperature ($T_6$) was decreased, from 150 to 125°C, and the $CO_2$ flow rate was increased, up to 2 ml $min^{-1}$, the foams produced become inhomogeneous. As observed in pure PMMA, one can distinguish two types of porosities in the blend foams, determined by their mean dimensions (e.g., for PMMA/10 wt% MAM_150_1.5 sample, $\emptyset_{large\ cell} \approx 200$ µm and $\emptyset_{small\ cell} \approx 40$ µm). This bimodality may be due to a limit of $CO_2$ dissolution in the polymer at given ($P$, $T$, $w_{CO_2}$) that creates heterogeneities.

With MAM addition, it is possible to further decrease the extruding temperatures below 130°C (which is the lowest temperature reached to foam pure PMMA). Under 125°C and down to 110°C in the die ($T_6$), the foams are homogeneous again and contain micro porosities ($40 \leq \emptyset_{cell} \leq 100$ µm). These cells tend to be oriented in the direction of extrusion and are not anymore spherical. In fact, below 125°C, the cells are more polyhedral than spherical.

In brief both pure PMMA (Figure 6) and PMMA/10 wt% MAM (Figure 7) foams produced through $scCO_2$-assisted extrusion process in this study are microcellular. However, due to MAM addition in the PMMA matrix, one can produce PMMA/10 wt% MAM foams at lower temperature than pure PMMA. Reducing the die temperature seems to have an impact on the porosity type (total porosity and open-porosity content) and homogeneity of cells (very regular cells especially at the lowest densities in presence of MAM). These aspects are detailed in the following part.

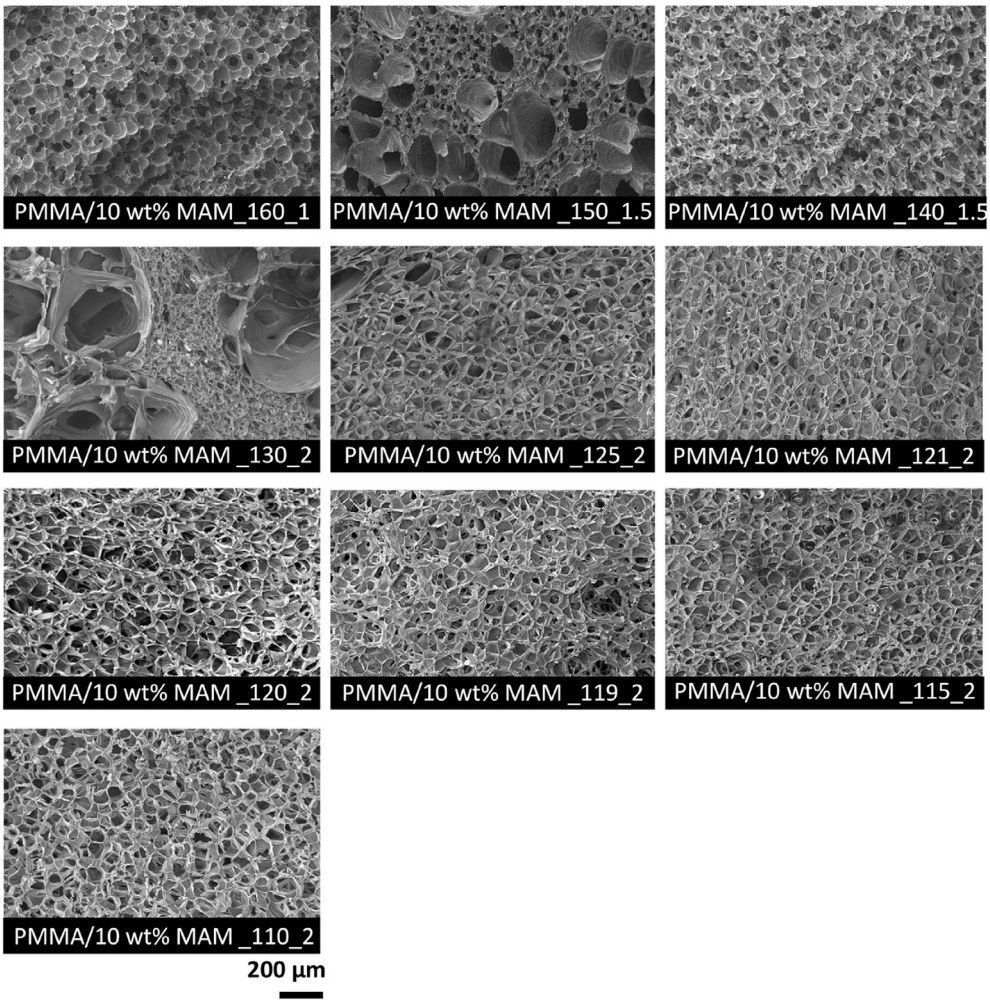


**FIGURE 7** SEM images (X200) of central area of neat PMMA/10 wt% MAM foams extruded in conditions detailed in Table 4

**TABLE 5** PMMA and PMMA/10 wt% MAM foams cell density ($N_C$) approximation

| | Low-density foams | | Mid-density foams | | High-density foams | |
|---|---|---|---|---|---|---|
| **Sample name** | **PMMA_130_2** | **PMMA/10 wt% MAM_125_2** | **PMMA_142_2** | **PMMA/10 wt% MAM _160_1** | **PMMA_171_0.7** | **//** |
| $\emptyset_{cell}$ (µm) | 80 or 100[a] | 65 | 55 | 40 | 150 | // |
| $\rho_f^{H_2O}$ (g cm$^{-3}$) | 0.06 | 0.04 | 0.3 | 0.25 | 0.65 | // |
| note N° $N_c$ (cells cm$^{-3}$) | 3.6 to 7 × 10$^7$[a] | 20 × 10$^7$[b] | 3.4 × 10$^7$[c] | 10 × 10$^7$[d] | 0.05 × 10$^7$[e] | //[f] |

[a]Very heterogeneous foam, lowest density, obtained at the lowest extrusion temperature, $\emptyset_{cell}$ ranging from 50 to 200 µm; $N_C$ value is estimated by using average $\emptyset_{cell}$ values, respectively equal to 80 or 100 µm.
[b]Homogeneous foam of lowest density, not necessarily obtained at the lowest temperature, average $\emptyset_{cell}$ of 65 µm is used.
[c]Rather homogeneous foam, obtained at an in-between extrusion temperature.
[d]Homogeneous foam, obtained at the highest extrusion temperature.
[e]Heterogeneous foam, obtained at the highest extrusion temperature, $\emptyset_{cell}$ average is taken at 150 µm.
[f]A high density close to 0.65 g cm$^{-3}$ cannot be achieved with the blend PMMA/10 wt% MAM.

### 3.3.3 | PMMA and PMMA/10 wt% MAM foams cell density

In spite of the heterogeneity of the pore distribution and the presence of large pores, the pore nucleation density ($N_c$) has been evaluated following Equation (9). In the case of a double population, an approximate mean cell diameter ($\emptyset_{cell}$) was taken around the mid value. Then we varied this value to test the sensitivity of the resulting $N_c$. The values of mean cell size may not represent reality

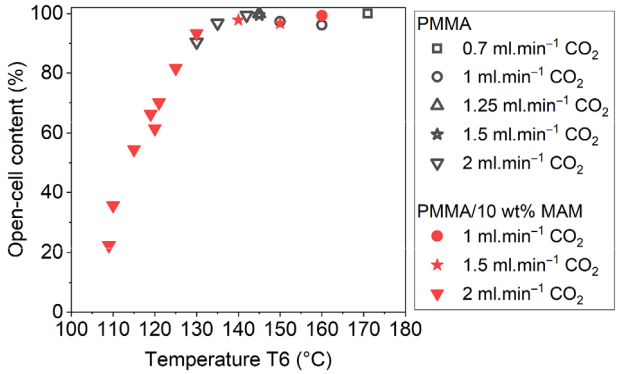


**FIGURE 8** Evolution of the open cell content in samples foamed at given die temperature ($T_6$) with a specific amount of $scCO_2$ [Color figure can be viewed at wileyonlinelibrary.com]

(it does not take into account the distribution of cells diameter) but provide a simple way to evaluate the cell density. The results compiled in Table 5 compare the cells densities of PMMA and blend foams of nearly comparable densities.

Comparing columns 2 by 2 (Table 5) at nearly comparable density, the effect of MAM appears by an increase of cells density. However, the order of magnitude of micellar objects density in the dense blend is not yet achieved (order of magnitude: $10^{14}$ micelles $cm^{-3}$ in the literature).[14,17] Indeed, the material does not vitrify quickly enough to stop the coalescence. Further work is in progress to enhance the cell density and tend to produce foams with a higher cell density.

## 3.4 | Foam open-cell content

As shown in Figure 8, in both PMMA and PMMA/10 wt % MAM blend, the open-cell content is maximum (100 ± 5%) and exhibits a plateau over a temperature range of 35°C (between 170 and 135°C).

Then, looking at behavior when the die temperature is decreased away from the plateau (from 160 to 109°C for the blend), the open cell-content decreases (from 100% to 22% for the blend). This phenomenon is more visible with the example of the blend because the die temperature was reduced on a wide range (from 160 to 109°C). Indeed, after a temperature threshold (on the high temperature side), open-cell content decreases.

Chauvet et al. observed the same trend with PLA foams (*i.e.*, after a temperature threshold the open-cell content decreases when die temperature is decreased).[22,28] This tendency is linked to the material stiffening. Indeed, when the die temperature is reduced, coalescence and cell connections are limited; so the cell walls cannot collapse to create open porosities.

# 4 | CONCLUSION

Pure PMMA and PMMA/10 wt% foamed through $scCO_2$-assisted extrusion foaming. The lowering of extrusion die temperature balanced by an increase of $CO_2$ flow rate led to the production of very lightweight acrylic foams ($\rho = 0.05 g cm^{-3}$). The very low foams densities reached in extrusion are unique and had never been equaled in a discontinuous process macro or microcellular range. However, PMMA foams are not homogeneous and MAM addition is necessary to reach this homogeneity. For the first time, the efficiency of MAM as a foam homogenizer in liquid state foaming has been proved. MAM also acts as a foam structure controller and blend foams contain smaller porosities than neat PMMA foams. Concomitantly, in extruded foams of the very low-density range (<0.1 $g cm^{-3}$), an increase in cell density (up to 4 $10^8$ cells $cm^{-3}$) was achieved. However, the increase of the order of magnitude of cell density to $10^{15}$ or $10^{16}$ cells $cm^{-3}$ for extrusion nano foaming is not yet achieved.

## AUTHORS CONTRIBUTION

**Martial Sauceau:** Conceptualization (lead); data curation (supporting); formal analysis (supporting); investigation (lead); methodology (lead); supervision (supporting); writing – original draft (supporting). **Fabien Baillon:** Conceptualization (supporting); data curation (supporting); formal analysis (supporting); investigation (supporting); supervision (supporting); validation (supporting); writing – original draft (supporting). **Louise Le Barbenchon:** Data curation (supporting); investigation (supporting); methodology (equal); visualization (equal); writing – original draft (supporting). **Matthieu Pedros:** Data curation (supporting). **Michel Dumon:** Conceptualization (lead); data curation (supporting); formal analysis (equal); funding acquisition (lead); investigation (supporting); methodology (supporting); project administration (lead); supervision (lead); validation (lead); writing – original draft (supporting). **Margaux Haurat:** Formal analysis (lead); investigation (equal); writing – original draft (lead).

## ACKNOWLEDGMENTS

This work was supported by the Agence Nationale de la Recherche (ANR, France) (AAPG PRCE 2018CE06 0030, 2019); ANR is gratefully acknowledged.

## DATA AVAILABILITY STATEMENT

Research data are not shared.

## ORCID

*Margaux Haurat* https://orcid.org/0000-0001-7988-3528

## REFERENCES


[1] D. H. Everett, *Manual of Symbols and Terminology for Physicochemical Quantities and Units*, IUPAC Division of Physical Chemistry, Washington DC **1971**.
[2] M. Haurat, M. Dumon, *Molecules* **2020**, *25*, 5320.
[3] B. Notario, J. Pinto, E. Solorzano, J. A. de Saja, M. Dumon, M. A. Rodríguez-Pérez, *Polymer* **2015**, *56*, 57.
[4] E. Di Maio, E. Kiran, *J. Supercrit. Fluids* **2018**, *134*, 157.
[5] S. Liu, J. Duvigneau, G. J. Vancso, *Eur. Polym. J.* **2015**, *65*, 33.
[6] V. Bernardo, J. Martin-de Leon, J. Pinto, U. Schade, M. A. Rodriguez-Perez, *Colloids Surf. A Physicochem. Eng. Asp.* **2020**, *600*, 124937.
[7] G. Coste, C. Negrell, S. Caillol, *Eur. Polym. J.* **2020**, *140*, 110029.
[8] B. Krause, H. J. P. Sijbesma, P. Münüklü, N. F. A. van der Vegt, M. Wessling, *Macromolecules* **2001**, *34*, 8792.
[9] S. P. Nalawade, F. Picchioni, L. P. B. M. Janssen, *Prog. Polym. Sci.* **2006**, *31*, 25.
[10] S. K. Goel, E. J. Beckman, *Polym. Eng. Sci.* **1994**, *34*, 1137.
[11] J. M. León, V. Bernardo, M. Á. Rodríguez-Pérez, *Macromol. Mater. Eng.* **2017**, *302*, 5.
[12] J. Pinto, J. A. Reglero-Ruiz, M. Dumon, M. A. Rodriguez-Perez, *J. Supercrit. Fluids* **2014**, *94*, 198.
[13] S. Pérez-Tamarit, B. Notario, E. Solórzano, M. A. Rodriguez-Perez, *Mater. Lett.* **2018**, *210*, 39.
[14] J. Pinto, M. Dumon, M. Pedros, J. Reglero, M. A. Rodriguez-Perez, *Chem. Eng. J.* **2014**, *243*, 428.
[15] P. Spitael, C. W. Macosko, R. B. McClurg, *Macromolecules* **2004**, *37*, 6874.
[16] M. Dumon, J. A. R. Ruiz, J. P. Sanz, M. A. R. Perez, J.-M. Tallon, M. Pedros, E. Cloutet, P. Viot, *Cell. Polym.* **2012**, *31*, 207.
[17] V. Bernardo, J. Martin-de Leon, J. Pinto, T. Catelani, A. Athanassiou, M. A. Rodriguez-Perez, *Polymer* **2019**, *163*, 115.
[18] V. Bernardo, J. Martin-de Leon, E. Laguna-Gutierrez, T. Catelani, J. Pinto, A. Athanassiou, M. A. Rodriguez-Perez, *Polymer* **2018**, *153*, 262.
[19] L. Zhu, S. Costeux, K. A. Patankar, J. D. Moore, Nanocellular thermoplastic foam and process for making the same **2016**.
[20] S. Costeux, *J. Appl. Polym. Sci.* **2014**, *131*.
[21] J. A. R. Ruiz, M. Pedros, J.-M. Tallon, M. Dumon, *J. Supercrit. Fluids* **2011**, *58*, 168.
[22] M. Chauvet, M. Sauceau, F. Baillon, J. Fages, *J. Appl. Polym. Sci.* **2021**, *138*, 50150.
[23] M. Chauvet, M. Sauceau, J. Fages, *J. Supercrit. Fluids* **2017**, *120*, 408.
[24] N. L. Moigne, M. Sauceau, M. Benyakhlef, R. Jemai, J.-C. Bénézet, É. Rodier, J.-M. Lopez-Cuesta, J. Fages, *Eur. Polym. J.* **2014**, *61*.
[25] T. Vigh, M. Sauceau, J. Fages, E. Rodier, I. Wagner, P. L. Sóti, G. Marosi, Z. K. Nagy, *Polym. Adv. Technol.* **2014**, *25*, 1135.
[26] C. Nikitine, E. Rodier, M. Sauceau, J.-J. Letourneau, J. Fages, *J. Appl. Polym. Sci.* **2010**, *115*, 981.
[27] C. Nikitine, E. Rodier, M. Sauceau, J. Fages, *Chem. Eng. Res. Des.* **2009**, *87*, 809.
[28] M. Chauvet, M. Sauceau, F. Baillon, J. Fages, *J. Appl. Polym. Sci.* **2017**, *134*, 45067.
[29] NIST. https://webbook.nist.gov/chemistry/, **2022**.
[30] S. Costeux, D. Foether, Conf. Proc. Annual Tech. Conf.-ANTEC, Orlando **2015**, p. 2740.
[31] M. Haurat, T. Tassaing, M. Dumon, *J. Supercrit. Fluids* **2022**, *182*, 105534.
[32] C. B. Park, A. H. Behravesh, R. D. Venter, *Polym. Eng. Sci.* **1998**, *1812*, 38.
[33] J. Wang, W. Zhu, H. Zhang, C. B. Park, *Chem. Eng. Sci.* **2012**, *75*, 390.
[34] J. A. Reglero Ruiz, C. Saiz-Arroyo, M. Dumon, M. A. Rodríguez-Perez, L. Gonzalez, *Polym. Int.* **2011**, *60*, 146.
[35] H. E. Naguib, C. B. Park, U. Panzer, N. Reichelt, *Polym. Eng. Sci.* **2002**, *42*, 1481.
[36] H. E. Naguib, C. B. Park, N. Reichelt, *J. Appl. Polym. Sci.* **2004**, *91*, 2661.
[37] J. A. Reglero Ruiz, M. Dumon, J. Pinto, M. A. Rodriguez-Pérez, *Macromol. Mater. Eng.* **2011**, *296*, 752.
[38] H. Guo, A. Nicolae, V. Kumar, *Polymer* **2015**, *70*, 231.
[39] P. Gong, G. Wang, M.-P. Tran, P. Buahom, S. Zhai, G. Li, C. B. Park, *Carbon* **2017**, *120*, 1.
[40] C. Zhang, B. Zhu, D. Li, L. J. Lee, *Polymer* **2012**, *53*, 2435.


## SUPPORTING INFORMATION

Additional supporting information can be found online in the Supporting Information section at the end of this article.

**How to cite this article:** M. Haurat, M. Sauceau, F. Baillon, L. L. Barbenchon, M. Pedros, M. Dumon, *J. Appl. Polym. Sci.* **2022**, e53277. https://doi.org/10.1002/app.53277